Search for Invisible Decays of a Dark Photon Produced in e^+e^- Collisions at BABAR

J. P. Lees,[1] V. Poireau,[1] V. Tisserand,[1] E. Grauges,[2] A. Palano,[3] G. Eigen,[4] D. N. Brown,[5] M. Derdzinski,[5] A. Giuffrida,[5] Yu. G. Kolomensky,[5] M. Fritsch,[6] H. Koch,[6] T. Schroeder,[6] C. Hearty,[7a,7b] T. S. Mattison,[7b] J. A. McKenna,[7b] R. Y. So,[7b] V. E. Blinov,[8a,8b,8c] A. R. Buzykaev,[8a] V. P. Druzhinin,[8a,8b] V. B. Golubev,[8a,8b] E. A. Kravchenko,[8a,8b] A. P. Onuchin,[8a,8b,8c] S. I. Serednyakov,[8a,8b] Yu. I. Skovpen,[8a,8b] E. P. Solodov,[8a,8b] K. Yu. Todyshev,[8a,8b] A. J. Lankford,[9] J. W. Gary,[10] O. Long,[10] A. M. Eisner,[11] W. S. Lockman,[11] W. Panduro Vazquez,[11] D. S. Chao,[12] C. H. Cheng,[12] B. Echenard,[12] K. T. Flood,[12] D. G. Hitlin,[12] J. Kim,[12] T. S. Miyashita,[12] P. Ongmongkolkul,[12] F. C. Porter,[12] M. Röhrken,[12] Z. Huard,[13] B. T. Meadows,[13] B. G. Pushpawela,[13] M. D. Sokoloff,[13] L. Sun,[13,†] J. G. Smith,[14] S. R. Wagner,[14] D. Bernard,[15] M. Verderi,[15] D. Bettoni,[16a] C. Bozzi,[16a] R. Calabrese,[16a,16b] G. Cibinetto,[16a,16b] E. Fioravanti,[16a,16b] I. Garzia,[16a,16b] E. Luppi,[16a,16b] V. Santoro,[16a] A. Calcaterra,[17] R. de Sangro,[17] G. Finocchiaro,[17] S. Martellotti,[17] P. Patteri,[17] I. M. Peruzzi,[17] M. Piccolo,[17] M. Rotondo,[17] A. Zallo,[17] S. Passaggio,[18] C. Patrignani,[18,‡] H. M. Lacker,[19] B. Bhuyan,[20] U. Mallik,[21] C. Chen,[22] J. Cochran,[22] S. Prell,[22] H. Ahmed,[23] A. V. Gritsan,[24] N. Arnaud,[25] M. Davier,[25] F. Le Diberder,[25] A. M. Lutz,[25] G. Wormser,[25] D. J. Lange,[26] D. M. Wright,[26] J. P. Coleman,[27] E. Gabathuler,[27,*] D. E. Hutchcroft,[27] D. J. Payne,[27] C. Touramanis,[27] A. J. Bevan,[28] F. Di Lodovico,[28] R. Sacco,[28] G. Cowan,[29] Sw. Banerjee,[30] D. N. Brown,[30] C. L. Davis,[30] A. G. Denig,[31] W. Gradl,[31] K. Griessinger,[31] A. Hafner,[31] K. R. Schubert,[31] R. J. Barlow,[32,§] G. D. Lafferty,[32] R. Cenci,[33] A. Jawahery,[33] D. A. Roberts,[33] R. Cowan,[34] S. H. Robertson,[35] B. Dey,[36a] N. Neri,[36a] F. Palombo,[36a,36b] R. Cheaib,[37] L. Cremaldi,[37] R. Godang,[37,¶] D. J. Summers,[37] P. Taras,[38] G. De Nardo,[39] C. Sciacca,[39] G. Raven,[40] C. P. Jessop,[41] J. M. LoSecco,[41] K. Honscheid,[42] R. Kass,[42] A. Gaz,[43a] M. Margoni,[43a,43b] M. Posocco,[43a] G. Simi,[43a,43b] F. Simonetto,[43a,43b] R. Stroili,[43a,43b] S. Akar,[44] E. Ben-Haim,[44] M. Bomben,[44] G. R. Bonneaud,[44] G. Calderini,[44] J. Chauveau,[44] G. Marchiori,[44] J. Ocariz,[44] M. Biasini,[45a,45b] E. Manoni,[45a] A. Rossi,[45a] G. Batignani,[46a,46b] S. Bettarini,[46a,46b] M. Carpinelli,[46a,46b,**] G. Casarosa,[46a,46b] M. Chrzaszcz,[46a] F. Forti,[46a,46b] M. A. Giorgi,[46a,46b] A. Lusiani,[46a,46c] B. Oberhof,[46a,46b] E. Paoloni,[46a,46b] M. Rama,[46a] G. Rizzo,[46a,46b] J. J. Walsh,[46a] A. J. S. Smith,[47] F. Anulli,[48a] R. Faccini,[48a,48b] F. Ferrarotto,[48a] F. Ferroni,[48a,48b] A. Pilloni,[48a,48b] G. Piredda,[48a,*] C. Bünger,[49] S. Dittrich,[49] O. Grünberg,[49] M. Heß,[49] T. Leddig,[49] C. Voß,[49] R. Waldi,[49] T. Adye,[50] F. F. Wilson,[50] S. Emery,[51] G. Vasseur,[51] D. Aston,[52] C. Cartaro,[52] M. R. Convery,[52] J. Dorfan,[52] W. Dunwoodie,[52] M. Ebert,[52] R. C. Field,[52] B. G. Fulsom,[52] M. T. Graham,[52] C. Hast,[52] W. R. Innes,[52] P. Kim,[52] D. W. G. S. Leith,[52] S. Luitz,[52] D. B. MacFarlane,[52] D. R. Muller,[52] H. Neal,[52] B. N. Ratcliff,[52] A. Roodman,[52] M. K. Sullivan,[52] J. Va'vra,[52] W. J. Wisniewski,[52] M. V. Purohit,[53] J. R. Wilson,[53] A. Randle-Conde,[54] S. J. Sekula,[54] M. Bellis,[55] P. R. Burchat,[55] E. M. T. Puccio,[55] M. S. Alam,[56] J. A. Ernst,[56] R. Gorodeisky,[57] N. Guttman,[57] D. R. Peimer,[57] A. Soffer,[57] S. M. Spanier,[58] J. L. Ritchie,[59] R. F. Schwitters,[59] J. M. Izen,[60] X. C. Lou,[60] F. Bianchi,[61a,61b] F. De Mori,[61a,61b] A. Filippi,[61a] D. Gamba,[61a,61b] L. Lanceri,[62] L. Vitale,[62] F. Martinez-Vidal,[63] A. Oyanguren,[63] J. Albert,[64] A. Beaulieu,[64b] F. U. Bernlochner,[64b] G. J. King,[64b] R. Kowalewski,[64b] T. Lueck,[64b] I. M. Nugent,[64b] J. M. Roney,[64b] R. J. Sobie,[64a,64b] N. Tasneem,[64b] T. J. Gershon,[65] P. F. Harrison,[65] T. E. Latham,[65] R. Prepost,[66] and S. L. Wu[66]

(BABAR Collaboration)

[1]*Laboratoire d'Annecy-le-Vieux de Physique des Particules (LAPP), Université de Savoie, CNRS/IN2P3, F-74941 Annecy-Le-Vieux, France*
[2]*Universitat de Barcelona, Facultat de Fisica, Departament ECM, E-08028 Barcelona, Spain*
[3]*INFN Sezione di Bari and Dipartimento di Fisica, Università di Bari, I-70126 Bari, Italy*
[4]*University of Bergen, Institute of Physics, N-5007 Bergen, Norway*
[5]*Lawrence Berkeley National Laboratory and University of California, Berkeley, California 94720, USA*
[6]*Ruhr Universität Bochum, Institut für Experimentalphysik 1, D-44780 Bochum, Germany*
[7a]*Institute of Particle Physics, Vancouver, British Columbia V6T 1Z1, Canada*
[7b]*University of British Columbia, Vancouver, British Columbia V6T 1Z1, Canada*
[8a]*Budker Institute of Nuclear Physics SB RAS, Novosibirsk 630090, Russia*
[8b]*Novosibirsk State University, Novosibirsk 630090, Russia*
[8c]*Novosibirsk State Technical University, Novosibirsk 630092, Russia*
[9]*University of California at Irvine, Irvine, California 92697, USA*
[10]*University of California at Riverside, Riverside, California 92521, USA*
[11]*University of California at Santa Cruz, Institute for Particle Physics, Santa Cruz, California 95064, USA*
[12]*California Institute of Technology, Pasadena, California 91125, USA*
[13]*University of Cincinnati, Cincinnati, Ohio 45221, USA*

[14]*University of Colorado, Boulder, Colorado 80309, USA*
[15]*Laboratoire Leprince-Ringuet, Ecole Polytechnique, CNRS/IN2P3, F-91128 Palaiseau, France*
[16a]*INFN Sezione di Ferrara, I-44122 Ferrara, Italy*
[16b]*Dipartimento di Fisica e Scienze della Terra, Università di Ferrara, I-44122 Ferrara, Italy*
[17]*INFN Laboratori Nazionali di Frascati, I-00044 Frascati, Italy*
[18]*INFN Sezione di Genova, I-16146 Genova, Italy*
[19]*Humboldt-Universität zu Berlin, Institut für Physik, D-12489 Berlin, Germany*
[20]*Indian Institute of Technology Guwahati, Guwahati, Assam 781 039, India*
[21]*University of Iowa, Iowa City, Iowa 52242, USA*
[22]*Iowa State University, Ames, Iowa 50011, USA*
[23]*Physics Department, Jazan University, Jazan 22822, Saudi Arabia*
[24]*Johns Hopkins University, Baltimore, Maryland 21218, USA*
[25]*Laboratoire de l'Accélérateur Linéaire, IN2P3/CNRS et Université Paris-Sud 11,
Centre Scientifique d'Orsay, F-91898 Orsay Cedex, France*
[26]*Lawrence Livermore National Laboratory, Livermore, California 94550, USA*
[27]*University of Liverpool, Liverpool L69 7ZE, United Kingdom*
[28]*Queen Mary, University of London, London E1 4NS, United Kingdom*
[29]*University of London, Royal Holloway and Bedford New College, Egham, Surrey TW20 0EX, United Kingdom*
[30]*University of Louisville, Louisville, Kentucky 40292, USA*
[31]*Johannes Gutenberg-Universität Mainz, Institut für Kernphysik, D-55099 Mainz, Germany*
[32]*University of Manchester, Manchester M13 9PL, United Kingdom*
[33]*University of Maryland, College Park, Maryland 20742, USA*
[34]*Massachusetts Institute of Technology, Laboratory for Nuclear Science, Cambridge, Massachusetts 02139, USA*
[35]*Institute of Particle Physics and McGill University, Montréal, Québec H3A 2T8, Canada*
[36a]*INFN Sezione di Milano, I-20133 Milano, Italy*
[36b]*Dipartimento di Fisica, Università di Milano, I-20133 Milano, Italy*
[37]*University of Mississippi, University, Mississippi 38677, USA*
[38]*Université de Montréal, Physique des Particules, Montréal, Québec H3C 3J7, Canada*
[39]*INFN Sezione di Napoli and Dipartimento di Scienze Fisiche, Università di Napoli Federico II, I-80126 Napoli, Italy*
[40]*NIKHEF, National Institute for Nuclear Physics and High Energy Physics, NL-1009 DB Amsterdam, Netherlands*
[41]*University of Notre Dame, Notre Dame, Indiana 46556, USA*
[42]*The Ohio State University, Columbus, Ohio 43210, USA*
[43a]*INFN Sezione di Padova, I-35131 Padova, Italy*
[43b]*Dipartimento di Fisica, Università di Padova, I-35131 Padova, Italy*
[44]*Laboratoire de Physique Nucléaire et de Hautes Energies, IN2P3/CNRS, Université Pierre et Marie Curie-Paris 6,
Université Denis Diderot-Paris 7, F-75252 Paris, France*
[45a]*INFN Sezione di Perugia, I-06123 Perugia, Italy*
[45b]*Dipartimento di Fisica, Università di Perugia, I-06123 Perugia, Italy*
[46a]*INFN Sezione di Pisa, I-56127 Pisa, Italy*
[46b]*Dipartimento di Fisica, Università di Pisa, I-56127 Pisa, Italy*
[46c]*Scuola Normale Superiore di Pisa, I-56127 Pisa, Italy*
[47]*Princeton University, Princeton, New Jersey 08544, USA*
[48a]*INFN Sezione di Roma, I-00185 Roma, Italy*
[48b]*Dipartimento di Fisica, Università di Roma La Sapienza, I-00185 Roma, Italy*
[49]*Universität Rostock, D-18051 Rostock, Germany*
[50]*Rutherford Appleton Laboratory, Chilton, Didcot, Oxon OX11 0QX, United Kingdom*
[51]*CEA, Irfu, SPP, Centre de Saclay, F-91191 Gif-sur-Yvette, France*
[52]*SLAC National Accelerator Laboratory, Stanford, California 94309 USA*
[53]*University of South Carolina, Columbia, South Carolina 29208, USA*
[54]*Southern Methodist University, Dallas, Texas 75275, USA*
[55]*Stanford University, Stanford, California 94305, USA*
[56]*State University of New York, Albany, New York 12222, USA*
[57]*School of Physics and Astronomy, Tel Aviv University, Tel Aviv, 69978, Israel*
[58]*University of Tennessee, Knoxville, Tennessee 37996, USA*
[59]*University of Texas at Austin, Austin, Texas 78712, USA*
[60]*University of Texas at Dallas, Richardson, Texas 75083, USA*
[61a]*INFN Sezione di Torino, I-10125 Torino, Italy*
[61b]*Dipartimento di Fisica, Università di Torino, I-10125 Torino, Italy*
[62]*INFN Sezione di Trieste and Dipartimento di Fisica, Università di Trieste, I-34127 Trieste, Italy*
[63]*IFIC, Universitat de Valencia-CSIC, E-46071 Valencia, Spain*

[64a]*Institute of Particle Physics, Victoria, British Columbia, V8W 3P6, Canada*
[64b]*University of Victoria, Victoria, British Columbia, V8W 3P6, Canada*
[65]*Department of Physics, University of Warwick, Coventry CV4 7AL, United Kingdom*
[66]*University of Wisconsin, Madison, Wisconsin 53706, USA*

We search for single-photon events in 53 fb^{-1} of e^+e^- collision data collected with the *BABAR* detector at the PEP-II *B*-Factory. We look for events with a single high-energy photon and a large missing momentum and energy, consistent with production of a spin-1 particle A' through the process $e^+e^- \rightarrow \gamma A'$; $A' \rightarrow$ invisible. Such particles, referred to as "dark photons," are motivated by theories applying a $U(1)$ gauge symmetry to dark matter. We find no evidence for such processes and set 90% confidence level upper limits on the coupling strength of A' to e^+e^- in the mass range $m_{A'} \leq 8$ GeV. In particular, our limits exclude the values of the A' coupling suggested by the dark-photon interpretation of the muon $(g-2)_\mu$ anomaly, as well as a broad range of parameters for the dark-sector models.

The nature of dark matter is one of the greatest mysteries of modern physics. It is transparent to electromagnetic radiation and we have only been able to infer its existence through gravitational effects. Since terrestrial searches for dark-matter interactions have so far yielded null results, it is postulated to interact very weakly with ordinary matter. Recently, models attempting to explain certain astrophysical observations [1–4] as well as the muon $(g-2)_\mu$ anomaly [5] have introduced an appealing idea of a low-mass spin-1 particle, referred to as A' or U, that would possess a gauge coupling of electroweak strength to dark matter, but with a much smaller coupling to the standard model (SM) hypercharge [6,7]. Such a boson may be associated with a $U(1)$ gauge symmetry in the dark sector and kinetically mix with the SM photon with a mixing strength $\varepsilon \ll 1$, hence the name "dark photon." Values as high as $\varepsilon \sim 10^{-3}$ and masses in a GeV range have been predicted in the literature [6,7].

The decay modes of the dark photon depend on its mass and couplings, as well as on the particle spectrum of the dark sector. If the lowest-mass dark matter state χ is sufficiently light, $m_\chi < m_{A'}/2$, then the dominant decay mode of the A' is invisible, $A' \rightarrow \chi\bar{\chi}$. The cleanest collider signature of such particles is the production of monochromatic single photons in $e^+e^- \rightarrow \gamma A'$, accompanied by significant missing energy and momentum. The photon energy E_γ^* in the e^+e^- center-of-mass (c.m.) is related to the missing mass M_X through $M_X^2 = s - 2E_\gamma^*\sqrt{s}$, where s is the square of the c.m. energy, and the asterisk hereafter denotes a c.m. quantity. We seek a signal of the dark photon A' as a narrow peak in the distribution of M_X^2 in events with a single high-energy photon. As expected for the dark matter coupling $\alpha_D < 1$ [7], we assume that the decay width of the A' is negligible compared to the experimental resolution, and that the A' decays predominantly to dark matter (i.e., the invisible branching fraction is $\approx$100%). Furthermore, we assume that a single A' state exists in the range

$0 < m_{A'} \leq 8$ GeV, or if two or more states are present, they do not interfere.

The current best limits on the mixing strength ε of the dark photon are from searches for narrow peaks in the e^+e^- or $\mu^+\mu^-$ invariant mass spectra [8–14] and from beam-dump and neutrino experiments [15,16]. These limits assume that the dominant decays of the A' are to the visible SM particles, but are not valid if there are low-mass invisible degrees of freedom. There are constraints on invisible decays of the A' from kaon decays [17–19] and from the recent search for missing energy events in electron-nucleus scattering [20].

We search for the process $e^+e^- \rightarrow \gamma A'$, followed by invisible decays of the A' in a 53 fb^{-1} data set [21] collected with the *BABAR* detector at the PEP-II asymmetric-energy e^+e^- collider at the SLAC National Accelerator Laboratory. The data were collected in 2007–2008 with c.m. energies near the $\Upsilon(2S)$, $\Upsilon(3S)$, and $\Upsilon(4S)$ resonances with a special "single-photon" trigger described below. The e^+e^- c.m. frame was boosted relative to the detector approximately along the detector's magnetic field axis by $\beta_z \approx 0.5$. Since the production of the A' is not expected to be enhanced by the presence of the Υ resonances, we combine the data sets collected in the vicinity of each Υ resonance. In order to properly account for acceptance effects and changes in the cross section as a function of $\sqrt{s}$, we measure the signal event yields separately for the $\Upsilon(2S)$, $\Upsilon(3S)$, and $\Upsilon(4S)$ data sets.

Since the *BABAR* detector is described in detail elsewhere [22], only the components of the detector crucial to this analysis are summarized below. Charged particle tracking is provided by a five-layer double-sided silicon vertex tracker and a 40-layer drift chamber (DCH). Photons and neutral pions are identified and measured using the electromagnetic calorimeter (EMC), which comprises 6580 thallium-doped CsI crystals. These systems are mounted inside a 1.5-T solenoidal superconducting magnet. The Instrumented Flux Return (IFR) forms the return yoke of the

superconducting coil, instrumented in the central barrel region with limited streamer tubes for the identification of muons and the detection of clusters produced by neutral hadrons. We use the GEANT4 [23] software to simulate interactions of particles traversing the *BABAR* detector, taking into account the varying detector conditions and beam backgrounds.

Detection of low-multiplicity single-photon events requires dedicated trigger lines. Event processing and selection proceeds in three steps. First, the hardware-based level-1 ($L1$) trigger accepts single-photon events if they contain at least one EMC cluster with energy above 800 MeV (in the laboratory frame). Second, $L1$-accepted events are forwarded to a software-based level-3 ($L3$) trigger, which forms DCH tracks and EMC clusters and makes decisions for a variety of physics signatures. Two single-photon $L3$ trigger lines were active during the data-taking period. The high-energy photon line (low M_X, hereafter "LowM") requires an isolated EMC cluster with energy $E_\gamma^* > 2$ GeV, and no tracks originating from the e^+e^- interaction region (IR). The LowM data set amounts to 5.9 fb^{-1} collected at the $\Upsilon(4S)$ resonance ($\sqrt{s} = 10.58$ GeV), 28.5 fb^{-1} collected at the $\Upsilon(3S)$ resonance ($\sqrt{s} = 10.36$ GeV), 2.7 fb^{-1} collected 30 MeV below the $\Upsilon(3S)$ resonance, 14.4 fb^{-1} collected at the $\Upsilon(2S)$ resonance ($\sqrt{s} = 10.02$ GeV), and 1.5 fb^{-1} collected 30 MeV below the $\Upsilon(2S)$ resonance. The total data sample collected with the LowM triggers is 53 fb^{-1}.

A low-energy (high M_X, "HighM") $L3$ single-photon trigger, which requires an EMC cluster with energy $E_\gamma^* > 1$ GeV and no tracks originating from the e^+e^- interaction region, was active for a subset of the data: 20 fb^{-1} collected at the $\Upsilon(3S)$ resonance as well as all of the data collected below the $\Upsilon(3S)$ and at the $\Upsilon(2S)$ resonances. The total data sample collected with the HighM triggers is 35.9 fb^{-1}.

Additional off-line software filters are applied to the stored data. We accept single-photon events if they satisfy one of the two following criteria. The LowM selection requires one EMC cluster in the event with $E_\gamma^* > 3$ GeV and no DCH tracks with momentum $p^* > 1$ GeV. The HighM selection requires one EMC cluster with the transverse profile consistent with an electromagnetic shower and $E_\gamma^* > 1.5$ GeV, and no DCH tracks with momentum $p^* > 0.1$ GeV. The two selection criteria are not mutually exclusive.

The trigger and reconstruction selections naturally split the data set into two broad M_X ranges. The LowM selections are used for the low-M_X region $-4 < M_X^2 < 36$ GeV^2. The backgrounds in this region are dominated by the QED process $e^+e^- \to \gamma\gamma$, especially near $M_X \approx 0$ ($E_\gamma^* \approx \sqrt{s}/2$). Because of the orientation of the EMC crystals, which point towards the IR, one of the photons may escape detection even if it is within the nominal EMC acceptance. The event selection is optimized to reduce this peaking background as much as possible. The HighM

trigger selection defines the high-M_X range $24 < M_X^2 < 69(63.5)$ GeV^2 for the $\Upsilon(3S)$ [$\Upsilon(2S)$] data set. This region is dominated by the low-angle radiative Bhabha events $e^+e^- \to e^+e^-\gamma$, in which both the electron and the positron escape the detector.

We suppress the SM backgrounds, which involve one or more particles that escape detection, by requiring that a candidate event be consistent with a single isolated photon shower in the EMC. We accept photons in the polar angle range $|\cos\theta_\gamma^*| < 0.6$, rejecting radiative Bhabha events that strongly peak in the forward and backward directions, and we require that the event contain no charged particle tracks.

The signal events are further selected by a multivariate boosted decision tree (BDT) discriminant [24], based on the following 12 discriminating variables. First, after a relatively coarse selection, we include the EMC variables that describe the shape of the electromagnetic shower: the difference between the number of crystals in the EMC cluster and the expectation for a single photon of given energy, and two transverse shower moments [25]. Second, we include both the total excess EMC energy in the laboratory frame not associated with the highest-energy photon, and the c.m. energy and polar angle of the second-most-energetic EMC cluster. We also compute the azimuthal angle difference $\Delta\phi_{12}$ between the highest- and second-highest-energy EMC clusters; the $e^+e^- \to \gamma\gamma$ events with partial energy deposit in the EMC tend to peak at $\Delta\phi_{12} \sim \pi$. Third, a number of variables improve containment of the background events. We extrapolate the missing momentum vector to the EMC face, and compute the distance [in (θ, ϕ) polar lab-frame coordinates] to the nearest crystal edge. This allows us to suppress $e^+e^- \to \gamma\gamma$ events where one of the photons penetrates the EMC between crystals leaving little detectable energy. Furthermore, we look for energy deposited in the IFR, and compute the correlation angle $\Delta\phi_{NH}$ between the primary photon and the IFR cluster closest to the missing momentum direction; $e^+e^- \to \gamma\gamma$ events produce a peak at $\cos\Delta\phi_{NH} \sim -1$. We also apply a fiducial selection to the azimuthal angle ϕ_{miss} of the missing momentum by including $\cos(6\phi_{\text{miss}})$ into the BDT. This accounts for uninstrumented regions between six IFR sectors [22]. Finally, $\cos\theta_\gamma^*$ is included in the BDT to take advantage of the different angular distributions for signal and background events.

The BDT discriminants are trained separately in LowM and HighM regions. Each BDT is trained using 2.5×10^4 simulated signal events with uniformly distributed A' masses, and 2.5×10^4 background events from the $\Upsilon(3S)$ on-peak sample that corresponds to approximately 3 fb^{-1}. We test the BDT, define the final selection, and measure the signal efficiency using sets of 2.5×10^4 signal and background events statistically independent from the BDT training samples. The BDT score is designed so that the signal peaks near 1 while the background events are generally distributed between $-1 < \text{BDT} < 0$.

TABLE I.   Data sets and event selections used in this Letter. The characteristic energies of each data set are listed in rows; the event selections described in the text in columns. The table entries list the integrated luminosity and the numbers of events selected by each data set.

Data set		LowM				HighM	
Data set	$\mathcal{L}$	Selection			$\mathcal{L}$	Selection	
		$\mathcal{R}_B$	$\mathcal{R}'_L$	$\mathcal{R}_T$		$\mathcal{R}_B$	$\mathcal{R}_L$
$\Upsilon(2S)$	15.9 fb^{-1}	22,590	42	6	15.9 fb^{-1}	405,441	324
$\Upsilon(3S)$	31.2 fb^{-1}	68,476	129	26	22.3 fb^{-1}	719,623	696
$\Upsilon(4S)$	5.9 fb^{-1}	7,893	16	9			

The event selection is optimized to minimize the expected upper limit on the $e^+e^- \to \gamma A'$ cross section $\sigma_{A'}$. Since the number of peaking $e^+e^- \to \gamma\gamma$ events cannot be reliably estimated and has to be determined from the fit to the data, this background limits the sensitivity to $e^+e^- \to \gamma A'$ at the low A' masses where the photon energies for the two types of events are indistinguishable. In this regime, we define a "tight" selection region $\mathcal{R}_T$ which maximizes the ratio ε_S/N_B for large N_B, and $\varepsilon_S/2.3$ in the limit $N_B \to 0$, where ε_S is the selection efficiency for the signal and N_B is the number of background events expected in the full data sample. We also require $-0.4 < \cos\theta^*_\gamma < 0.6$ in order to suppress $e^+e^- \to \gamma\gamma$ events in which one of the photons would have missed the central region of the EMC.

A "loose" selection region $\mathcal{R}_L$ maximizes $\varepsilon_S/\sqrt{N_B}$. This selection is appropriate at higher M_X where the background is well described by a featureless continuum distribution, and maximal $\varepsilon_S/\sqrt{N_B}$ corresponds to the lowest upper limit on the $e^+e^- \to \gamma A'$ cross section.

Finally, a background region $\mathcal{R}_B$ is defined by $-0.5 <$ BDT < 0 and is used to determine the M_X^2 distribution of the background events. The selection criteria used in this analysis and the numbers of events selected in different datasets are summarized in Table I.

We measure the cross section $\sigma_{A'}$ as a function of the assumed mass $m_{A'}$ by performing a series of unbinned extended maximum likelihood fits to the distribution of M_X^2. For each value of $m_{A'}$, varied from 0 to 8.0 GeV in 166 steps roughly equal to half of the mass resolution, we perform a set of simultaneous fits to $\Upsilon(2S)$, $\Upsilon(3S)$, and for the low-M_X region, $\Upsilon(4S)$ data sets. Moreover, we subdivide the data into broad event selection bins: $\mathcal{R}_B$, used to define the background probability density functions (PDFs), and signal regions $\mathcal{R}_L$ (used for $5.5 < m_{A'} \le 8.0$ GeV), $\mathcal{R}_T$, and $\mathcal{R}'_L$ (used for $m_{A'} \le 5.5$ GeV). The region $\mathcal{R}'_L$ is defined to be the part of $\mathcal{R}_L$ not overlapping with $\mathcal{R}_T$. Thus, the simultaneous fits are performed to nine independent samples for $m_{A'} \le 5.5$ GeV, and four independent samples for $5.5 < m_{A'} \le 8.0$ GeV (missing mass spectra for all data sets are shown in [26]).

For the fits to the $\mathcal{R}_B$ regions, we fix the number of signal events to zero, and determine the parameters of the background PDFs. In the fits to the $\mathcal{R}_T$ and $\mathcal{R}'_L$ regions, we fix the background PDF shape, and vary the number of background events N_B, the number of peaking background events $e^+e^- \to \gamma\gamma$ (for $m_{A'} \le 5.5$ GeV), and the A' mixing strength ε^2. The numbers of signal and background events are constrained: $\varepsilon^2 \ge 0$ and $N_B > 0$.

The signal PDF is described by a Crystal Ball [27] function centered around the expected value of $M_X^2 = m_{A'}^2$. We determine the PDF as a function of $m_{A'}$ using high-statistics simulated samples of signal events, and we correct it for the difference between the photon energy resolution function in data and simulation using a high-statistics $e^+e^- \to \gamma\gamma$ sample in which one of the photons converts to an e^+e^- pair in the detector material [28]. The resolution for signal events decreases monotonically from $\sigma(M_X^2) = 1.5$ GeV^2 for $m_{A'} \approx 0$ to $\sigma(M_X^2) = 0.7$ GeV^2 for $m_{A'} = 8$ GeV. The background PDF has two components, a peaking background from $e^+e^- \to \gamma\gamma$ events, described by a Crystal Ball function, and a smooth function of M_X^2 dominated by the radiative Bhabha process $e^+e^- \to \gamma e^+e^-$ (second-order polynomial for $m_{A'} \le 5.5$ and a sum of exponentiated polynomials for $5.5 < m_{A'} \le 8.0$ GeV).

The signal selection efficiency varies slowly as a function of $m_{A'}$ between 2.4%–3.1% ($\mathcal{R}_T$ selection for $m_{A'} \le 5.5$ GeV), 3.4%–3.8% ($\mathcal{R}'_L$ for $m_{A'} \le 5.5$ GeV), and 2.0%–0.2% ($\mathcal{R}_L$ selection for $5.5 < m_{A'} \le 8.0$ GeV).

The largest systematic uncertainties in the signal yield are from the shape of the signal and background PDFs, and the uncertainties in the efficiency of signal and trigger selections. We determine the uncertainty in the signal PDF by comparing the data and simulated distributions of $e^+e^- \to \gamma\gamma$ events. We correct for the small observed differences, and use half of the correction as an estimate of the systematic uncertainty. We measure the trigger selection efficiency using single-photon $e^+e^- \to \gamma\gamma$ and $e^+e^- \to e^+e^-\gamma$ events that are selected from a sample of unbiased randomly accepted triggers. We find good agreement with
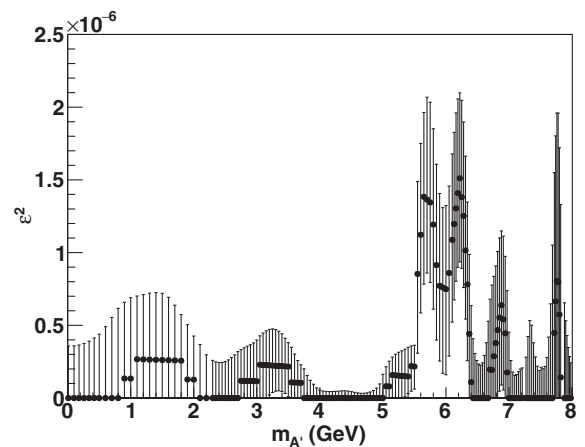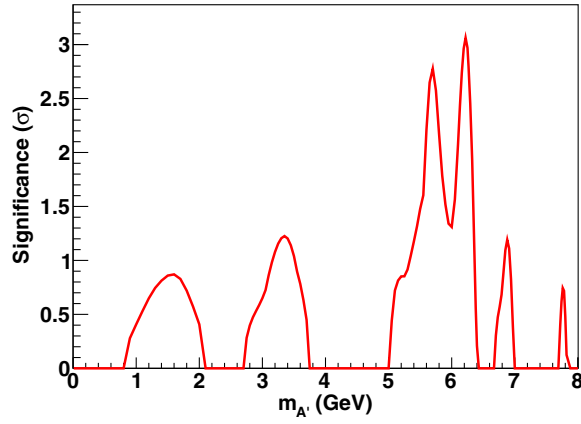

FIG. 1.   Measured maximum-likelihood values of the A' mixing strength squared ε^2 as a function of the mass $m_{A'}$.

FIG. 2.   Signal significance $\mathcal{S}$ as a function of the mass $m_{A'}$.

the simulation estimates of the trigger efficiency, within the systematic uncertainty of 0.4%. We compare the input BDT observables in simulation and in a sample of the single-photon data events, counting the difference as a systematic uncertainty of the signal selection efficiency. The total multiplicative error on the signal cross section is 5%, and is small compared to the statistical uncertainty.

Figure 1 shows the maximum-likelihood estimators of the A' mixing strength ε^2 for the 166 $m_{A'}$ hypotheses. The values of "local" significance of observation $\mathcal{S} \equiv \sqrt{2 \ln(L_{\max}/L_0)}$, where $L_{\max}$ is the maximum value of the likelihood, and L_0 is the value of the likelihood with the signal yield fixed to zero, are shown in Fig. 2. The most significant deviation of ε^2 from zero occurs at $m_{A'} = 6.21$ GeV and corresponds to $\mathcal{S} = 3.1$. Parametrized simulations determine that the probability to find such a
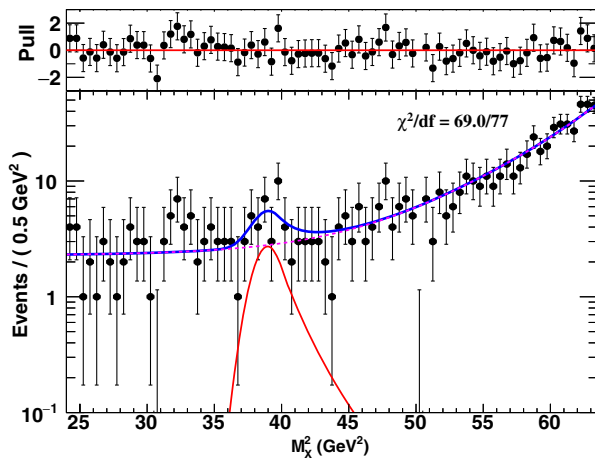
FIG. 3.   Bottom: Signal fit for $m_{A'} = 6.21$ GeV to a combination of $\Upsilon(2S)$ and $\Upsilon(3S)$ data sets, shown for illustration purposes. The signal peak (red) corresponds to the local significance $\mathcal{S} = 3.1$ (global significance of 2.6σ). Blue solid line shows the full PDF, while the magenta dashed line corresponds to the background contribution. Top: Distribution of the normalized fit residuals (pulls).
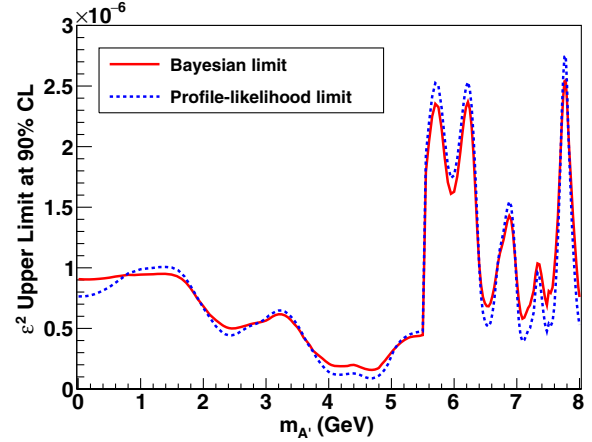
FIG. 4.   Upper limits at 90% C.L. on A' mixing strength squared ε^2 as a function of $m_{A'}$. Shown are the Bayesian limit computed with a uniform prior for $\varepsilon^2 > 0$ (solid red line) and the profile-likelihood limit (blue dashed line).

deviation in any of the 166 $m_{A'}$ points in the absence of any signal is $\approx 1\%$, corresponding to a "global" significance of 2.6σ. A representative fit for $m_{A'} = 6.21$ GeV is shown in Fig. 3.

The 90% confidence level (C.L.) upper limits on ε^2 as a function of $m_{A'}$ are shown in Fig. 4. We compute both the Bayesian limits with a uniform prior for $\varepsilon^2 > 0$ and the frequentist profile-likelihood limits [29]. Figure 5 compares our results to other limits on ε in channels where A' is allowed to decay invisibly, as well as to the region of parameter space consistent with the $(g-2)_\mu$ anomaly [5]. At each value of $m_{A'}$ we compute a limit on ε as a square root of the Bayesian limit on ε^2 from Fig. 4. Our data rule out the dark-photon coupling as the explanation for the $(g-2)_\mu$ anomaly. Our limits place stringent constraints on
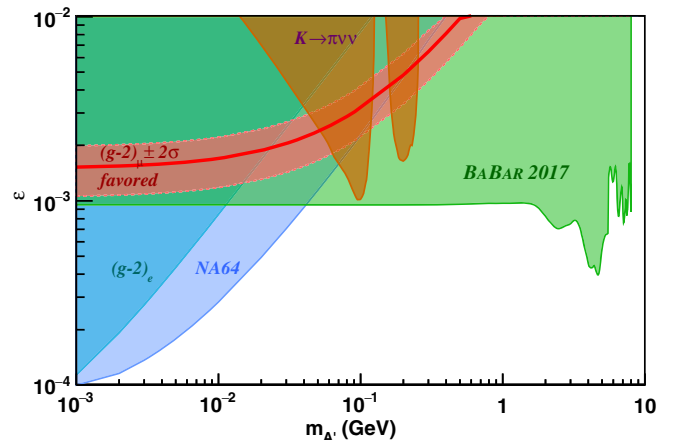

FIG. 5.   Regions of the A' parameter space (ε vs $m_{A'}$) excluded by this work (green area) compared to the previous constraints [7,18–20] as well as the region preferred by the $(g-2)_\mu$ anomaly [5].

dark-sector models over a broad range of parameter space, and represent a significant improvement over previously available results.

---

[*]Deceased.

[†]Present address: Wuhan University, Wuhan 43072, China.

[‡]Present address: Università di Bologna and INFN Sezione di Bologna, I-47921 Rimini, Italy.

[§]Present address: University of Huddersfield, Huddersfield HD1 3DH, United Kingdom.

[¶]Present address: University of South Alabama, Mobile, Alabama 36688, USA.

[**]Also at Università di Sassari, I-07100 Sassari, Italy.

[1] P. Jean *et al.*, Astron. Astrophys. **407**, L55 (2003); J. Knodlseder *et al.*, Astron. Astrophys. **411**, L457 (2003).

[2] O. Adriani *et al.* (PAMELA Collaboration), Nature (London) **458**, 607 (2009).

[3] M. Ackermann *et al.* (Fermi LAT Collaboration), Phys. Rev. Lett. **108**, 011103 (2012).

[4] Z. Berezhiani, A. D. Dolgov, and I. I. Tkachev, Eur. Phys. J. C **73**, 2620 (2013).

[5] G. W. Bennett *et al.* (Muon $g-2$ Collaboration), Phys. Rev. D **73**, 072003 (2006).

[6] P. Fayet, Phys. Lett. **95B**, 285 (1980); Nucl. Phys. **B187**, 184 (1981); B. Holdom, Phys. Lett. **166B**, 196 (1986);

[7] R. Essig *et al.*, arXiv:1311.0029, and references therein.

[8] J. P. Lees *et al.* (*BABAR* Collaboration), Phys. Rev. Lett. **113**, 201801 (2014).

[9] D. Babusci *et al.* (KLOE-2 Collaboration), Phys. Lett. B **720**, 111 (2013); **736**, 459 (2014).

[10] J. R. Batley *et al.* (NA48/2 Collaboration), Phys. Lett. B **746**, 178 (2015).

[11] P. Adlarson *et al.* (WASA-at-COSY Collaboration), Phys. Lett. B **726**, 187 (2013).

[12] G. Agakishiev *et al.* (HADES Collaboration), Phys. Lett. B **731**, 265 (2014).

[13] H. Merkel *et al.* (A1 Collaboration), Phys. Rev. Lett. **112**, 221802 (2014).

[14] S. Abrahamyan *et al.* (APEX Collaboration), Phys. Rev. Lett. **107**, 191804 (2011).

[15] J. Blümlein and J. Brunner, Phys. Lett. B **731**, 320 (2014).

[16] S. Andreas, C. Niebuhr, and A. Ringwald, Phys. Rev. D **86**, 095019 (2012).

[17] M. Pospelov, Phys. Rev. D **80**, 095002 (2009).

[18] S. Adler *et al.* (E787 Collaboration), Phys. Rev. Lett. **88**, 041803 (2002).

[19] A. V. Artamonov *et al.* (E949 Collaboration), Phys. Rev. D **79**, 092004 (2009).

[20] D. Banerjee *et al.* (NA64 Collaboration), Phys. Rev. Lett. **118**, 011802 (2017).

[21] J. P. Lees *et al.* (*BABAR* Collaboration), Nucl. Instrum. Methods Phys. Res., Sect. A **726**, 203 (2013).

[22] B. Aubert *et al.* (*BABAR* Collaboration), Nucl. Instrum. Methods Phys. Res., Sect. A **479**, 1 (2002); **729**, 615 (2013).

[23] S. Agostinelli *et al.* (GEANT4 Collaboration), Nucl. Instrum. Methods Phys. Res., Sect. A **506**, 250 (2003).

[24] A. Hoecker *et al.*, *Proc. Sci.*, ACAT2007 (2007) 040 [arXiv: physics/0703039].

[25] A. Drescher, B. Gräwe, B. Hahn, B. Ingelbach, U. Matthiesen, H. Scheck, J. Spengler, and D. Wegener (ARGUS Collaboration), Nucl. Instrum. Methods Phys. Res., Sect. A **237**, 464 (1985).

[26] See Supplemental Material at http://link.aps.org/supplemental/10.1103/PhysRevLett.119.131804 for additional plots.

[27] M. J. Oreglia, Ph. D. thesis, Stanford University, 1980, Appendix D; J. E. Gaiser, Ph. D. thesis, Stanford University, 1982, Appendix F; T. Skwarnicki, Ph. D. thesis, Cracow INP and DESY, 1986, Appendix E.

[28] P. del Amo Sanchez *et al.* (*BABAR* Collaboration), Phys. Rev. Lett. **107**, 021804 (2011).

[29] W. A. Rolke, A. M. Lopez, and J. Conrad, Nucl. Instrum. Methods Phys. Res., Sect. A **551**, 493 (2005).